Freie Universität Berlin

Title: Modifying the Magnetic Anisotropy of an Iron Porphyrin Molecule by an on-Surface Ring-Closure Reaction

Author(s): Arruda, L. M., Ali, Md. E., Bernien, M., Nickel, F., Kopprasch, J., Czekelius, C., … Kuch, W.

Document type: Postprint

Modifying the Magnetic Anisotropy of an Iron Porphyrin Molecule by an On-Surface Ring-Closure Reaction

Lucas M. Arruda,[1,2,*] Md. Ehesan Ali,[3] Matthias Bernien,[1] Fabian Nickel,[1] Jens Kopprasch,[1] Constantin Czekelius,[4] Peter M. Oppeneer,[5] and Wolfgang Kuch[1]

[1]*Institut für Experimentalphysik, Freie Universität Berlin,*
Arnimallee 14, 14195 Berlin, Germany

[2]*CAPES Foundation, Ministry of Education of Brazil, 70040-020 Brasília-DF, Brazil*

[3]*Institute of Nano Science and Technology,*
Phase-10, Sector-64, Mohali-160062, Punjab, India

[4]*Institut für Organische Chemie und Makromolekulare Chemie,*
Heinrich-Heine-Universität Düsseldorf,
Universitätsstraße 1, 40225 Düsseldorf, Germany

[5]*Department of Physics and Astronomy,*
Uppsala University, Box 516, 75120 Uppsala, Sweden

Abstract

The magnetic properties of adsorbed metalloporphyrin molecules can be altered or tuned by the substrate, additional axial ligands, or changes to the molecules' macrocycle. These modifications influence the electronic configuration of the fourfold-coordinated central metal ion that is responsible for the metalloporphyrins' magnetic properties. We report a substantial increase in the effective spin moment obtained from sum-rule analysis of X-ray magnetic circular dichroism (XMCD) for an iron metalloporphyrin molecule on Au(111) through its conversion from iron(II)-octaethylporphyrin (FeOEP) to iron(II)-tetrabenzoporphyrin (FeTBP) in a surface-assisted ring-closure ligand reaction. Density functional theory calculations with additional strong Coulomb correlation (DFT+U) show that the on-surface reaction alters the conformation of the molecule, increasing its planarity and the ion-surface distance. A spin-Hamiltonian fit of the magnetization as a function of field reveals a substantial increase in the intra-atomic magnetic dipole term (T_z) and a decrease in the magnitude of the easy-plane anisotropy upon ring closure. This consequence of the ring closure demonstrates how new magnetic properties can be obtained from on-surface reactions, resulting here in significant modifications to the magnetic anisotropy of the Fe ion, and sheds light onto the molecule-substrate interaction in these systems.

* larruda@physik.fu-berlin.de

I. INTRODUCTION

Great attention has been devoted in recent years to the study of molecular magnets, as their small size and chemical flexibility make them promising candidates for individual building blocks in spintronics. In this quickly developing field, the spin of the electrons is used in addition to their charge, for instance, in logic and storage devices. Molecules with high spin,[1–3] high magnetic anisotropy,[4,5] and slow magnetic relaxation[6,7] have been identified and their deposition mechanisms,[8,9] substrate-molecule[10–13] and intramolecular interactions[14–16] are subject of active research.

Iron porphyrin molecules, presented here, are among these studied molecules. They are metal-organic complexes consisting of a central Fe ion, responsible for the molecules' magnetic properties.[17] They were shown to generally deposit on crystal substrates in a mostly flat geometry and arrange themselves in well-ordered structures.[18,19] Their molecular structure favors at the same time the formation of stable heterostructures on surfaces and a strong bonding to the central ion, which is coordinated to the molecular macrocycle through four bonds with the nitrogen atoms, leaving two coordination sites available, above and below the metal ion. The site below the metal ion is usually occupied by the surface, contributing to the high stability of these compounds on surfaces, while the one above remains free to be occupied by additional ligands. The different ligands that can be attached to this free coordination site allow for a great number of possibilities in tuning the properties of the complex.[20–24] The addition of ligands is not the only cause of such variations, though, as modification of the macrocyclic ligands of the porphyrin also promotes changes in the properties of the central metal ion.[25,26]

An important property of magnetic systems is their magnetic anisotropy, given its significance to the interaction with external magnetic fields and the magnetic relaxation of these systems. As such, their manipulation is extremely interesting for the development of spintronic devices. The manipulation of magnetic anisotropy in molecules, two-dimensional supramolecular arrays at surfaces, and single atoms has been successfully achieved through different methods, such as on-surface reactions,[27] substrate coordination site selection,[28,29] and direct manipulation with a scanning tunneling microscope (STM) tip.[30,31] Oxygen adsorption has been shown to even promote the switching of the magnetic anisotropy axis in molecular arrays.[32] The magnetic anisotropy can be obtained by modeling magnetization

curves obtained for different directions of the magnetic field with a spin Hamiltonian and comparing it to the experimentally obtained curves.

On-surface reactions are a promising way of modifying molecules and obtaining new molecular arrangements, frequently difficult or impossible to obtain otherwise. These reactions are usually irreversible,[33,34] be it an intermolecular reaction that forms new covalently bound macrostructures or intramolecular reactions resulting in new covalent bonds within the molecules. This can be an advantage, but only when the reaction processes are understood to the point one can control them to the required level of precision. These reactions often change the conformation of a molecule or molecular array,[35–38] leading to different electronic and magnetic properties, and depend on several different aspects of the system environment. It has been shown that different thermal conditions lead to alternative results on a surface,[39] with intermolecular or intramolecular reactions being favored depending on the temperature of the substrate. The molecule-substrate interaction is another important factor. Experiments show that substrate atoms can act as components or catalysts of molecular reactions.[40–42] In the case of porphyrins, while the reactions and molecular arrangements of the molecules often do not depend on the central ion, the change caused by these factors and the substrate interaction affect strongly its magnetic and electronic properties.[43–46]

The use of X-ray magnetic circular dichroism (XMCD) as a probe for the magnetic properties of molecular systems is well established, but some care is still necessary when drawing conclusions from these experiments. Even though the element specificity of X-ray absorption (XA) is particularly efficient in isolating the properties of single elements of the molecule from other components, the individual contribution of the different molecular orbitals associated with that element and high degree of angle-dependent variation of the recorded signal demand careful analysis of the data. An important consequence of this affects the determination of the spin moment (m_S) of the system through the application of the sum rules.[47,48] What is obtained from XMCD is an effective spin moment (m_S^{eff}), which includes the angle-dependent intra-atomic magnetic dipole term (T_{z}). This term represents the spatial distribution of the spin density, usually increasing as the symmetry of the system is reduced. As such, it can become very significant in low-symmetry molecular systems.[49]

Understanding how the electronic, magnetic, and conformational properties of these molecules change is fundamental to the design of effective spintronic devices. In this work, a thermally induced intramolecular reaction of a metalloporphyrin molecule is studied by

X-ray absorption spectroscopy (XAS) and DFT+U calculations. In this reaction, described before in STM studies,[34,50] iron octaethylporphyrin (FeOEP) undergoes a dehydrogenation reaction in which ethyl groups form benzene rings, resulting in the iron tetrabenzoporphyrin (FeTBP) molecule, as shown schematically in Figure 1a. Significant changes are observed in the magnetic properties of the molecules resulting from this reaction, with striking modifications to the magnetic anisotropy of the Fe ion. The magnetic moments obtained from the experiment and the spin-Hamiltonian fit of the magnetization as a function of field are combined with density functional theory calculations to describe the magnetic state of the molecules.

II. METHODS

XAS and XMCD measurements. The XAS and XMCD measurements were taken at BESSY II, the Berlin Electron Storage Ring for Synchrotron Radiation, at the UE46_PGM-1 beamline. The beamline has a 10^{10} ph/s flux and the spot size was kept at $1\,\mathrm{mm}^2$ in order to have a less focused beam to help avoid radiation damage to the molecules. The energy resolution was set to $160\,\mathrm{meV}$. The signal was obtained by total electron yield and the data was normalized with the signal from a freshly evaporated Au grid placed upstream from the experiment. The measurements were taken at low temperatures of $4.5\,\mathrm{K}$, unless stated otherwise. The pressure in the magnet chamber was in the order of $2\cdot10^{-10}\,\mathrm{mbar}$, and the pressure in the preparation chamber was in the order of $1\cdot10^{-9}\,\mathrm{mbar}$. The XMCD measurements were taken with a field of $6\,\mathrm{T}$ in the direction of radiation incidence. The degree of circular polarization of the light was 85%. The molecules were synthesized as a dipyridine complex, $\mathrm{FeOEP(Py)_2}$. Samples were prepared under ultra-high vacuum by subliming the molecules from a Knudsen cell heated to a temperature of $500\,\mathrm{K}$ after 5 hours of degassing at $470\,\mathrm{K}$ to ensure the loss of the pyridine ligands. The molecules were deposited on a Au(111) substrate, cleaned beforehand by sputtering and annealing cycles, at room temperature to a submonolayer coverage of 0.9 ML. The coverage was checked with a quartz microbalance and crosschecked with intensity calibration of the iron, nitrogen, and carbon X-ray absorption edges normalized to the pre-edges.

DFT calculations. The density functional theory (DFT) calculations were performed at the generalized gradient approximation (GGA) level, employing for the GGA exchange-

correlation functional the parametrization of Perdew-Burke-Ernzerhof.[51] The calculations were carried out with the planewave-based Vienna ab-initio simulation package (VASP).[52] In addition, van der Waals dispersion interactions were taken into account through the Grimme D2 corrections.[53] The strong Coulomb correlations existing in the transition-metal $3d$-orbitals of the central metal ion were accounted for through on-site Hubbard U and exchange interactions J in the GGA+U approach.[54] Based on our previous experience,[11,55,56] we have chosen the U and J parameters as 4.0 and 1.0 eV, respectively. The projector augmented-wave (PAW) pseudopotentials[57] were used with a kinetic energy cutoff of 450 eV. Three layers of Au were considered to mimic the Au(111) substrate; this corresponds to a total of 300 Au atoms in the applied periodic simulation cell with dimensions $28.85 \times 24.98 \times 28.7$ Å^3. The on-surface optimizations of molecular geometries were performed by keeping the lowest atomic layers in their bulk unit cells position fixed and completely relaxing all other atomic positions. The reciprocal space was sampled using $2 \times 2 \times 1$ Monkhorst-Pack k-points.[58] The single-molecule geometries were optimized using the GGA+U method and the Γ point for the k-mesh. Lastly, we mention that the relativistic spin-orbit interaction has not been included in the present calculations, to keep the computational effort manageable.

III. RESULTS AND DISCUSSION

FeOEP molecules were deposited on a Au(111) surface with a coverage of 0.9 monolayers (ML). The ring-closure reaction was activated by annealing the sample to a temperature of 600 K. Nitrogen K edge spectra (Figure 1b) display a clear difference in the electronic structure of the molecules before and after the annealing process, evidencing the transition from FeOEP to FeTBP, as discussed by Heinrich et al.[34] While the first major peak at 398.8 eV seems to be fairly independent of the molecule's transition, the second peak is shifted to lower energies, and its overall intensity is diminished. The reduction in the signal intensity, also visible in the spectra for 54.7° incidence as shown in Figure S1 of the supporting information, indicates a charge transfer to the nitrogen atoms of the molecule.

The XAS of the Fe $L_{2,3}$ edge for two grazing incidence geometries, taken at 4.5 K, is presented in Figure 2. The electronic structure of the Fe center of the molecules is seen in this figure to be significantly changed by the annealing process, most notably by an energetic contraction of the Fe L_3 edges on the FeTBP for different incidence angles. The peak energies
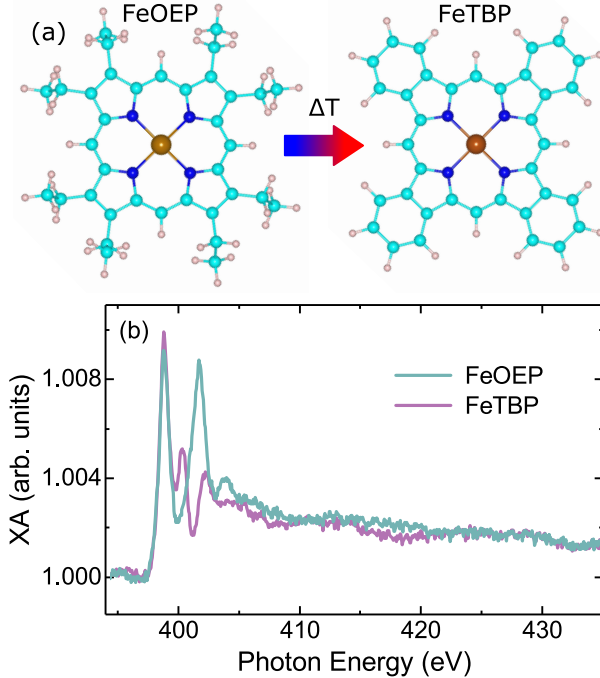
Figure 1: Top view of the DFT-optimized structures of FeOEP and FeTBP (a). Nitrogen K edge XA of FeOEP and FeTBP on Au(111) taken at room temperature and grazing incidence of the X-rays (b) displaying the difference in the line shape of the two molecules, characteristic of the ring-closure reaction.

are closer together in FeTBP, with the lower energy features shifting towards higher energies and the higher energy ones displaying a redshift with respect to FeOEP. This points to a direct contraction of the energy levels of the Fe ion due to ligand field reduction after ring closure. A small contraction of the energies of the states above the Fermi energy is indeed verified in the density of states (DOS) calculations to be presented shortly. The DOS results are also foreshadowed by the double-peak structure of the L_3 edge in the FeTBP molecule, and the triple-peak structure found in the FeOEP, particularly for the vertical polarization measurements. Analysis of the integrated intensity shows that there is an 8% decrease upon ring closure for 20° angle of incidence of horizontally polarized X-rays, while the integrated intensity for vertically polarized X-rays with the same incidence angle is increased by 2%. The charge density distribution is thus 10% more anisotropic after ring closure. For vertically polarized X-rays, the Fe in-plane orbitals are primarily probed at all incidence angles, while for horizontal polarization at grazing incidence the majority of the signal is from out-of-plane orbitals. Due to the small increase in the integrated intensity
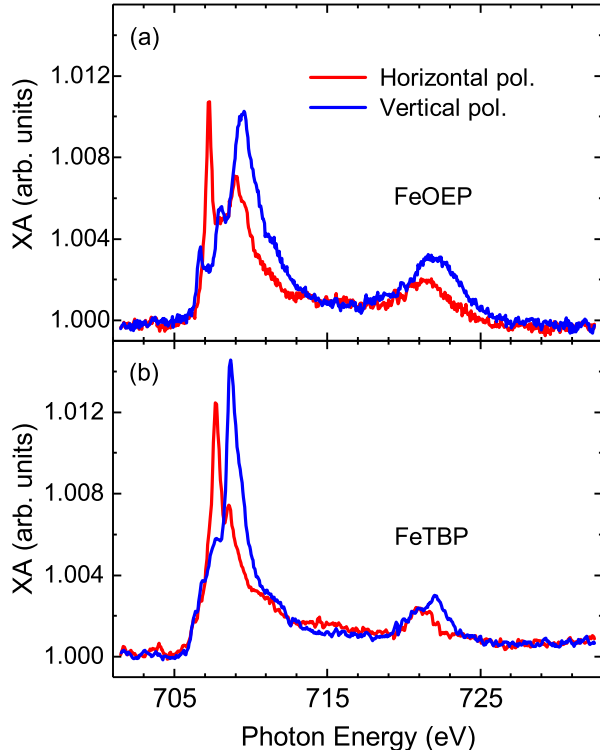
Figure 2: XA spectra of the Fe $L_{2,3}$ edges of FeOEP (a) and FeTBP (b) on Au(111) under $20°$ angle of incidence for horizontal and vertical linearly polarized X-rays and $T = 4.5\,\mathrm{K}$.

for vertical polarization, the differences in the spectral shape for the different molecules under this polarization are attributed to charge reorganization between different in-plane orbitals and energy level shifts. This and the stronger decrease in the integrated intensity for horizontal polarization points to a very small charge transfer from the out-of-plane orbitals of the Fe ion to its surroundings in FeOEP/Au, and to an increased overlap of its wave functions with the substrate. Interestingly, changes can be observed in the FeOEP spectra at higher temperatures even before the reaction takes place. Figure S4 of the supporting information shows the spectra of the OEP molecule at room temperature, where line shapes reminiscent of the FeTBP spectra are observed. These line shapes are only preserved for lower temperatures once the ring-closure reaction has taken place. Further investigation is required to fully understand this behavior.

The m_l- and spin-resolved DOS for free FeOEP and FeTBP have been computed using the DFT+U approach, adopting the generalized gradient approximation (GGA) for the exchange-correlation functional (see Methods). The calculated magnetic moments on the central Fe atoms are 1.96 and $2.09\,\mu_\mathrm{B}$, respectively, for single molecule FeOEP and FeTBP.

The total spin of both molecular species is thus $S \sim 1$. However, due to the differences in the ring structures, a significant difference is observed in the ordering of the $3d$ orbital energies (see Figure 3a and b). FeOEP is computed to have an electronic configuration as $(d_{xy})^2$, $(d_{z^2})^2$, $(d_{xz})^1$, $(d_{yz})^1$, $(d_{x^2-y^2})^0$, while for FeTBP it is $(d_{xy})^2$, $(d_{z^2})^1$, $\{(d_{xz}), (d_{yz})\}^3$, $(d_{x^2-y^2})^0$. These differences between the electronic structures of FeTBP and FeOEP are mainly due to the strained, non-planar macrocyclic structure of FeOEP caused by the eight ethyl groups attached to the porphyrin ring, whereas FeTBP has a planar ring structure (see Figure 1a for a top view of the structure). This difference in the ring structure is reflected in the m_l-resolved DOS for the central metal atom as well.

Considering next the molecules adsorbed on a Au(111) substrate, we observed a substantial change in the electronic structure of FeOEP when deposited on the Au substrate, even though we find that the molecule-substrate interactions are very weak in nature and mainly driven by non-bonded electrostatic interactions like the Van der Waals interaction. The distance between the Fe atom and the Au top layer is calculated as $2.53 \, \text{Å}$. This value is obtained when D2-type[53] dispersion interactions are taken into account. Without incorporating these dispersion interactions, the geometrical optimizations gave a much larger, unphysical distance (i.e. $\sim 5.0 \, \text{Å}$) between the molecule and the Au substrate. The optimized shorter distances give consequently a weak overlap of the charge densities of molecule and substrate and lead to a re-hybridization of the electronic states of FeOEP with respect to the free molecule, resulting in an altered electronic configuration on the Au(111) substrate (Figure 3c). However, there is little change in the structure parameters of FeOEP when deposited on the substrate. The major changes between the free molecule and FeOEP/Au(111) are observed in the d_{z^2} orbital occupation and hybridization, see Figure 3c. In the free molecule the d_{z^2} orbital is completely occupied, however, due to interaction with the substrate, the d_{z^2} DOS peak changes to a broad featureless DOS structure extending over $4 \, \text{eV}$. This reveals that the iron ion in FeOEP interacts with the Au substrate mainly through its d_{z^2} orbital.

We observed a quite similar behavior for the d_{z^2} orbital of FeTBP as well, when grafted on top of the Au(111) substrate. Additionally, one can observe a slight change in the unoccupied DOS peaks for the out-of-plane (d_{yz} and d_{xz}) orbitals, see Figure 3d. We further note an interesting feature, namely that the interaction through the d_{z^2} orbital of the molecule with the substrate is larger in FeOEP/Au(111) than in FeTBP/Au(111), as can be seen from the larger energy broadening of the d_{z^2}-orbital DOS of FeOEP upon adsorption on Au(111), as
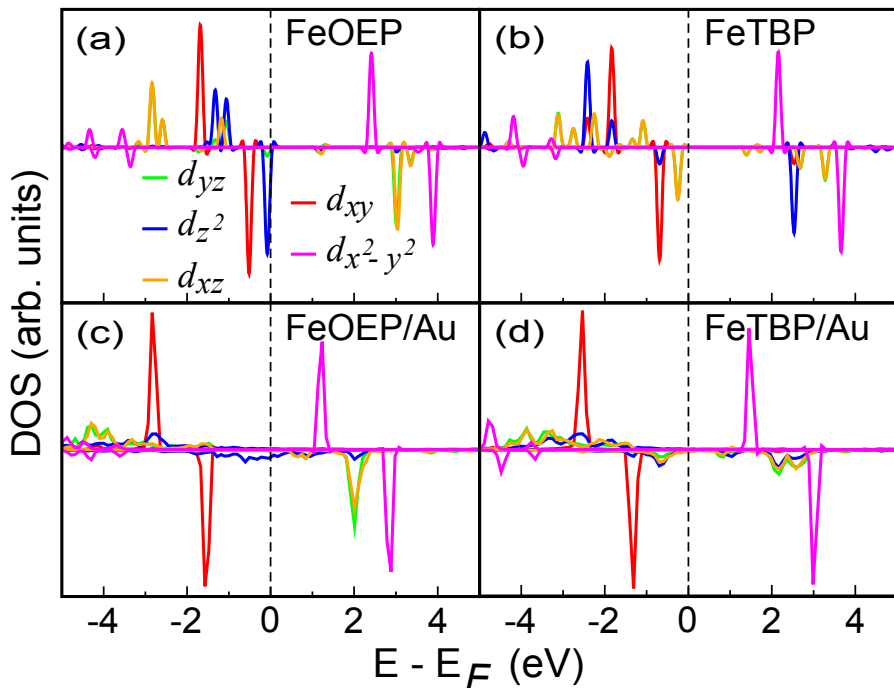
9

Figure 3: DFT+U-calculated $3d$-orbital DOS plots for single-molecule FeOEP (a) and FeTBP (b), and for molecules adsorbed on Au(111), FeOEP/Au (c), and FeTBP/Au (d). Positive and negative orbital DOS is for majority and minority spin, respectively.

compared to FeTBP. This can be related to the computed equilibrium distance between the Fe atom and the top Au layer, which is $2.88\,\text{Å}$ for FeTBP/Au, larger than that of FeOEP/Au. Thus, there is a possibility for electron transfer between the FeOEP and the substrate. As mentioned above, in gas-phase FeOEP the d_{z^2} orbital is completely filled and the broadened peak around the Fermi level for FeOEP/Au indicates strong interactions with the metallic Au substrate. Such electron transfer is not observed in the case of FeTBP/Au(111), where the d_{z^2} orbital is already half-filled in the free molecule. The on-surface ring-closure from FeOEP to FeTBP leads thus to a change of the local DOS of mainly the d_{z^2}-orbitals for minority spins which changes from a metallic DOS for FeOEP/Au to a non-metallic DOS for FeTBP/Au. The intensity of the out-of-plane $d_{\pi}(d_{xz}, d_{yz})$ orbitals reduces somewhat as these are influenced by the on-surface chemical reaction. The formation of the benzene rings on the FeTBP leads to a larger π-system on the ligands of the molecule, promoting greater interaction between them and the d_{π} orbitals of the iron ion. The electron density reorganization that results from these changes can be seen in the partial DOS of one of the C atoms of the terminal ethylene groups, shown in the supporting information (Figure S3).

10

The reduction in the intensity of these orbitals in the DOS can be then attributed to an increased interaction between them and the extended π-system of the ligands. Hybridization is also likely with the nitrogen atom, leading to the characteristic changes to the N K edge, seen in Figure 1b. This leads to a change of the average Fe–N distance from 1.995 to 2.013 Å from FeOEP to FeTBP, respectively.

Spin-density plots with the same isosurface value of $0.01\,\mu_{\mathrm{B}}/\text{Å}^3$ indicate that the electronic interactions associated with the unpaired orbitals occur through the central metal atom and the Au substrate atoms underneath (see Figure 4). Note that the existence of a spin density on the non-magnetic atom underneath a magnetic center not necessarily indicates the formation of chemical bonds, especially when the interaction is mainly governed by the van-der-Waals dispersion and electrostatic interactions, but there can be a slight spin polarization of Au orbitals and charge transfer (see, e.g. Reference 59). A stronger spin polarization and chemical bonding between Au surface atoms and an iron phthalocyanine molecule has previously been obtained with calculations based on the local spin density approximation (LSDA), which, however, predicted a shorter molecule-substrate distance.[60] The here-obtained $0.02\,\mu_{\mathrm{B}}$ magnetic moment on the Au atom underneath indicates fractional charge transfer to the central Fe atom of the FeOEP from the substrate (see Table 1). The shape of the spin density on the Fe atom for FeOEP/Au (Figure 4a) reflects the information from the calculated DOS, that the out-of-plane d_π orbitals are responsible for the magnetic properties while the d_{z^2} orbital makes a bond with the substrate. This is also seen in the computed electronic populations in the d-orbitals for FeOEP/Au, presented in Table S1 of the supporting information.

TABLE 1: Structural and Magnetic Properties of FeOEP/Au(111) and FeTBP/Au(111), Calculated with the DFT+U Method (at GGA-D2 Level). Given are the optimized Fe–Au atomic distances and spin moments.

GGA-D2 optimized properties	FeOEP/Au(111)	FeTBP/Au(111)
Fe–Au distance	2.67 Å	2.96 Å
spin moments (μ_{B}) on Fe	2.17 ($3d$)	2.01 ($3d$)
spin moments (μ_{B}) on attached Au	0.02 (total)	0.004 (total)

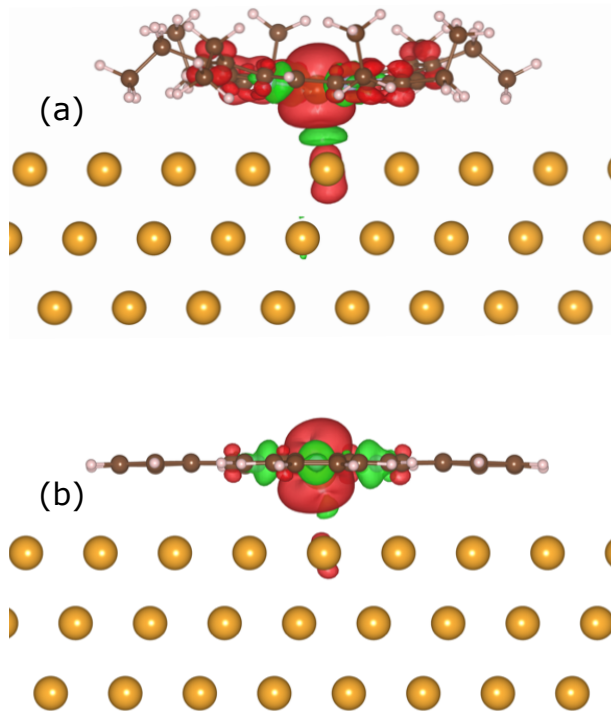The spin interaction of the two molecules with the substrate is seen to be tilted in Figure 4.

Figure 4: DFT+U-calculated spin densities for (a) FeOEP/Au(111) and (b) FeTBP/Au(111). The red and green spin density isosurface with isovalue of $0.01\,\mu_{\mathrm{B}}/\mathring{\mathrm{A}}^{3}$ indicate majority and minority spins.

This is caused by a displacement of the molecule on the surface, such that the Fe center does not sit on top of a Au atom. Although both molecules exhibit a displacement, the two positions are not exactly the same. In combination with the greater distance between Fe center and substrate (see Table 1), this promotes less interaction between Fe and the substrate and a reduction of the spin moments of both the Fe ion and the Au atoms underneath the molecules for the FeTBP. The asymmetric distortion of the d_{z^2} orbital seen in Figure 4b appears to also lead to more interaction and possibly hybridization with the d_π orbitals of the Fe, which would explain the greater affinity between these orbitals in Figure 3d.

Figure 5 shows the circular polarization XA and XMCD spectra of FeOEP and FeTBP for 20° and 90° angles of radiation incidence and external magnetic field directions. As seen in Figure 5c, the XMCD of FeOEP/Au for normal incidence is zero, which shows that the in-plane orbitals of the FeOEP molecule do not contribute to the magnetic moment, while the out-of-plane orbitals do, generating a clear XMCD signal under grazing incidence. For FeTBP/Au there is a small XMCD signal under normal incidence, and a significant increase
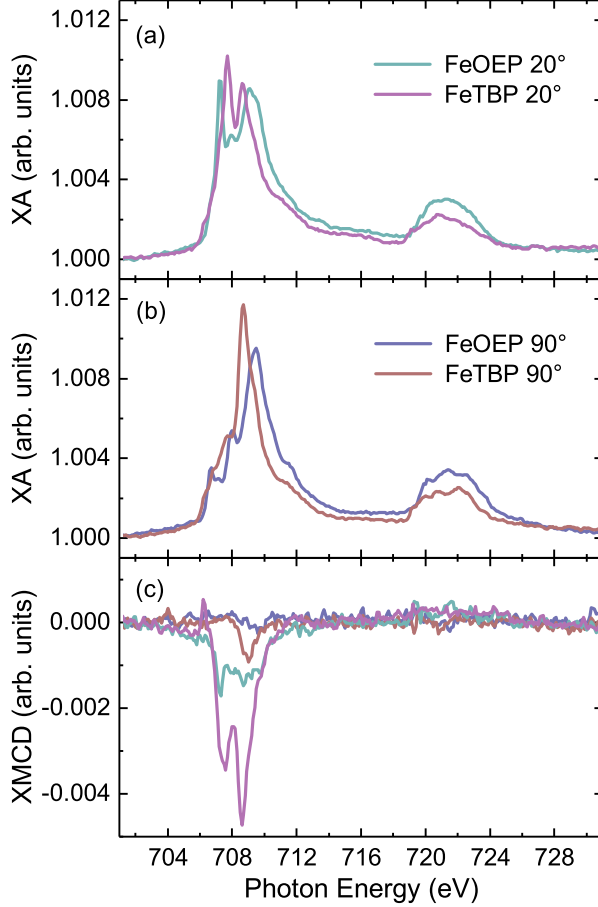
Figure 5: XA spectra of FeOEP and FeTBP on Au(111) under grazing (a) and normal (b) incidence of the circularly polarized X-rays, taken at an external field of $6\,T$ and temperature of $4.5\,K$, as well as the corresponding XMCD spectra (c).

under grazing incidence. These results and qualitative analysis of the angle dependence support the DFT+U results that in FeOEP/Au there are no half-filled in-plane orbitals, confirming that the magnetic signal obtained from this molecule under grazing incidence is due to out-of-plane orbitals.

The results of the sum-rule analysis[47,48] of the XMCD spectra are displayed in Table 2 for FeOEP/Au(111) and FeTBP/Au(111), assuming a $3d^6$ electronic configuration for both molecules. Here, $m_S^{\text{eff}}(\alpha)$ includes the T_z term contribution, except for the magic angle (35.3°), when it cancels out. The application of the sum rules provides values of 0.69(4) and 1.31(5) μ_B for the effective spin moment of FeOEP/Au and FeTBP/Au, respectively, under magic angle (35.3°) X-ray incidence and external field directions. These values are small when compared to the theoretical results because they are obtained from spectra taken

13

at 6 T and 4.5 K, far from magnetic saturation for either molecule, particularly for FeOEP, as will be shown in the following discussion of the magnetization curves. Additionally, the moments obtained from the sum rules will always be underestimated due to the limit of the sum-rules' applicability to lighter transition metal ions,[61] which introduces an intrinsic error to the sum-rule results for the magnetic moments of Fe. The errors in Table 2 only account for the noise of the spectra, and are therefore not representative of the real errors of the measurements.

TABLE 2: Results of the sum-rule analysis for the orbital and effective spin moment of FeOEP and FeTBP under three angles of incidence of the X-rays at 4.5 K and 6 T. The values have not been corrected for saturation.

	FeOEP		FeTBP	
α	$m_L(\alpha)/\mu_B$	$m_S^{\text{eff}}(\alpha)/\mu_B$	$m_L(\alpha)/\mu_B$	$m_S^{\text{eff}}(\alpha)/\mu_B$
90°	0.03 ± 0.02	-0.05 ± 0.07	0.07 ± 0.03	0.31 ± 0.07
35.3°	0.11 ± 0.02	0.69 ± 0.04	0.50 ± 0.02	1.31 ± 0.05
20°	0.18 ± 0.04	0.88 ± 0.05	0.70 ± 0.03	1.60 ± 0.06

The XMCD signal as a function of external magnetic field is displayed in Figure 6 for both molecules at grazing and normal incidence and field directions. The integrated values of the Fe L_3 edge (705 to 715 eV) XMCD signal, displayed as circles and diamonds, were taken from 0.2 to 6 T at a temperature of 4.5 K. To fit the lines, we used the following simplified spin Hamiltonian,

$$\mathcal{H} = \mu_\text{B} g \boldsymbol{B} \cdot \boldsymbol{S} + D S_\text{z}^2, \tag{1}$$

where only the Zeeman and the uniaxial anisotropy energy terms are considered. The first term represents the Zeeman energy (μ_B is Bohr's magneton, g is the g-factor, $\boldsymbol{B}$ is the external field vector and $\boldsymbol{S}$ is the spin vector), while the second one describes the uniaxial anisotropy energy (D is the zero-field-splitting parameter and S_z the spin component perpendicular to the plane of the molecule). Possible Kondo screening of the Fe moment, as suggested for FeTBP/Au(111) by an STM study,[34] as well as a contribution of the orbital magnetic moment to the Zeeman energy is approximately taken into account by treating g as a free fit parameter.
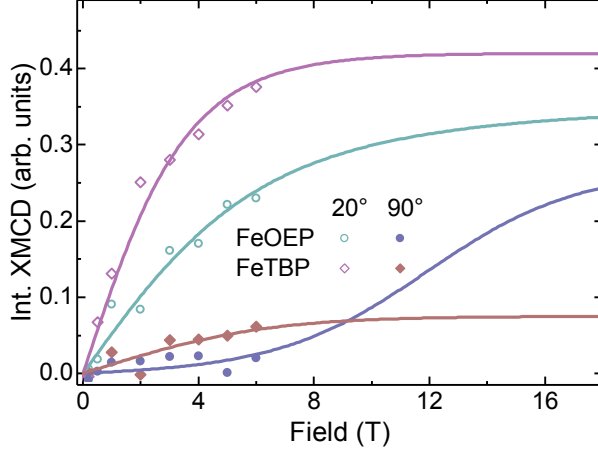
Figure 6: Experimental magnetization curves at $4.5\,\mathrm{K}$ of FeOEP and FeTBP (circles and diamonds, respectively) on Au(111) and corresponding spin-Hamiltonian fits (lines).

The moment obtained from this spin Hamiltonian is further modified by the intra-atomic magnetic dipole term (T_z). We need to consider the effective spin moment ($m_S^{\mathrm{eff}} = m_S - 7T_z(\cos^2\alpha - 2\sin^2\alpha)$, if the sample magnetization is in the same direction as the x-rays) for the signal obtained from the XMCD to be properly fitted. The influence of the (T_z) term will depend on the angle between the X-rays and the surface, α, and can be ignored for the magic angle of incidence, when $m_S^{\mathrm{eff}} = m_S$. Since the orbital moments obtained from the sum-rule analysis are larger for in-plane magnetization than for out-of-plane (Table 2), we restricted the fit to positive values of D, i.e., easy-plane anisotropy. With the spin calculated by DFT+U, $S = 1$, a meaningful fit of the experimental results can be obtained. It is shown in Figure 6 as solid lines. For the fit, $S = 1$ was fixed, and an upper limit for g was applied as $g = 2.5$, estimated from the sum-rule result for the orbital moment.

The effective spin moment is zero under normal incidence and magnetization direction if the value for T_z approaches its maximal negative value, $T_z = -m_S/14$ in this case, with m_S being the spin moment. The model used to fit the experimental magnetization curves is: $XMCD_{\mathrm{fit}} = a|m|\cos(\theta - \alpha)(1 + 7/(2m_S)T_z(1 - 3\cos(\theta + \alpha)/\cos(\theta - \alpha)))$, where a is the scaling to the experimental signal. In this generalized equation, θ is the angle of the sample magnetization to the surface, and $|m|\cos(\theta - \alpha)$ is the projection of the magnetization in the direction of the measurement. $(1 - 3\cos(\theta + \alpha)/\cos(\theta - \alpha))/4$ is the angle dependence of the T_z term. The T_z term is, thus, obtained from the fit. The magnetization is obtained from the spin-Hamiltonian equation. The scaling factor a to the experimental data was

fitted independently for FeOEP and FeTBP, but using the same scaling for normal- and grazing-incidence data.

The higher curvature of the magnetization curves of FeTBP/Au indicates that this system is closer to magnetic saturation than FeOEP/Au. From the fit one obtains that the FeOEP molecule on Au has a strong in-plane magnetic anisotropy ($D = 1.72$ meV) parallel to the plane of the molecule, while FeTBP/Au has a weaker anisotropy ($D = 0.39$ meV) in the same direction. In principle, relativistic calculations (including the spin-orbit interaction) could shed further light on the origin of the magnetic anisotropy, however, as mentioned before, they are out of the scope of the current work. For both molecules, g assumes the set limit of 2.5. From these fits, we thus do not see evidence for a Kondo screening of the Fe magnetic moment, which had been suggested by the STM study of Reference 34. On the other hand the presence of Kondo screening can also not be ruled out from the present XMCD data. Due to the number of free parameters used to describe the magnetization curves, the fits do not allow a definite statement about the absence or presence of Kondo screening. The fit furthermore reveals that the T_z term, which has a very low value of $-0.03\,\mu_B$ in FeOEP, increases by about four times to $-0.11\,\mu_B$ after ring closure. The fit of the magnetization curves reconciles the values obtained from the DFT+U calculations for the magnetic moments of the two molecules and what is observed in the XMCD results. The strong in-plane anisotropy of the FeOEP molecules almost quenches the magnetic signal observed in the XMCD for FeOEP/Au under normal incidence for lower fields, such as the maximum one measured in our experiments (6 T). The change in the intra-atomic magnetic dipole term is responsible for the increase in magnetic signal observed in grazing incidence after ring closure, when theory predicts no significant difference in the magnetic moment between the two molecules. The smaller XMCD signal in FeOEP/Au is, therefore, not a result of a smaller moment on this molecule, but of the different T_z and anisotropy terms. While the higher T_z term in FeTBP/Au should result in a decrease of the magnetic signal observed under normal incidence, this is balanced by the change in anisotropy. In FeTBP/Au, as can be seen in the spin density plots presented in Figure 4, the molecular conformation is much more planar than in FeOEP/Au. The flexibility of the ethyl groups of the OEP molecule allows for a conformation that distorts the molecular plane and brings the Fe center out of the plane of the molecule, closer to the substrate. This in turn enables a higher degree of interaction with the substrate and promotes the charge reorganization in the orbitals of the

OEP molecule in a more significant way than in TBP, as described in the DOS discussion.

With the parameters obtained from the fit of the magnetization curves, one can also estimate the saturation value expected for the magnetic moments at high field. The values obtained from the sum rules discussed previously can be adjusted by the estimated saturation factor obtained from the spin-Hamiltonian fit, yielding $1.1(3)\,\mu_B$ and $1.4(3)\,\mu_B$ under magic angle (35.3°) incidence and external field directions for the spin moment of the FeOEP and FeTBP, respectively, in magnetic saturation. In addition to the experimental error of this result, which accounts for the bending and noise of the $L_{2,3}$ edge spectra, there is an intrinsic error of about 20% in the magnetic moment value obtained from the sum-rule analysis due to the limit of its applicability to lighter transition metals.[61] This error is mainly due to the spectral overlap of the L_2 and L_3 edges for these ions. Considering these two main sources of error, the values obtained are in agreement with an $S = 1$ system, as predicted by DFT+U, and indicate that this is the most likely spin state for the two molecules. A second possibility, with $S = 3/2$, would require much higher values for the effective spin moment, and a third one, with $S = 1/2$, does not result in a meaningful fit of the magnetization curves with the spin-Hamiltonian model described previously. A last possibility would require an intermediary spin state, similar to the system described by Stepanow et $al.$[62] While this cannot be ruled out entirely just from the XMCD results, it is a very special scenario that is not supported by our DFT+U results. Inelastic excitations observed at about $\pm 7\,\mathrm{meV}$ in tunneling spectroscopy on FeOEP/Au(111)[34] suggest a much higher anisotropy ($D = \pm 7\,\mathrm{meV}$ for $S = 1$). As shown in Figure S8 in the supporting information, such a high value of D is not consistent with our experimental data and $S = 1$, since then the moments obtained from the sum-rule analysis and extrapolated to magnetic saturation would not match $S = 3/2$.

IV. CONCLUSIONS

The results have shown that the exploitation of intramolecular reactions on surfaces is a viable path to obtaining new molecules with suitable magnetic properties for their use in spintronics. Such reactions, although occurring at the periphery of the molecule, result in a significant change of the properties of the central metal ion. Additionally, a better understanding of the interactions between substrate and molecule is obtained from this study, a crucial step in the development of technologically suitable molecular magnets. The reaction

studied induces a conformational change in the molecule, causing not only a symmetry change in the molecular structure that induces a reduction of the ligand field splitting, but also bringing the metal center away from the substrate, further modifying it. The magnetic anisotropy of the iron ion is reduced by the ring closure reaction, contributing to a substantial increase in the effective magnetic spin moment obtained experimentally from XMCD under in-plane field direction. The different characteristics of the T_z term before and after the ring-closure reaction and the significant changes this causes to the effective spin moment of these systems illustrate how important the correct interpretation of the XMCD spectra and the treatment of the T_z-term contribution to these moments are.

Supporting Information. Magic angle N K edge XAS of the molecules before and after ring closure; N and C DOS plots; room temperature Fe $L_{2,3}$ edge XAS of FeOEP; magic angle Fe $L_{2,3}$ edge XMCD of FeOEP and FeTBP; example of the plots used for the sum-rule analysis; charge density plots of the two molecules on Au(111); calculated $3d$-orbital populations of the two molecules on Au(111); alternative fits of the magnetization curves with corresponding parameters; plot of the angle dependence of m_S^{eff} for FeOEP and FeTBP.

LIST OF REFERENCES

[1] Sessoli, R.; Tsai, H. L.; Schake, A. R.; Wang, S.; Vincent, J. B.; Folting, K.; Gatteschi, D.; Christou, G.; Hendrickson, D. N. High-Spin Molecules: $[Mn_{12}O_{12}(O_2CR)_{16}(H_2O)_4]$. *J. Am. Chem. Soc.* **1993**, *115*, 1804–1816.

[2] Kortus, J.; Baruah, T.; Bernstein, N.; Pederson, M. R. Magnetic Ordering, Electronic Structure, and Magnetic Anisotropy Energy in the High-Spin Mn_{10} Single Molecule Magnet. *Phys. Rev. B* **2002**, *66*, 092403.

[3] Herrera, J. M.; Marvaud, V.; Verdaguer, M.; Marrot, J.; Kalisz, M.; Mathonière, C. Reversible Photoinduced Magnetic Properties in the Heptanuclear Complex $[Mo^{IV}(CN)_2(CN–CuL)_6]^{8+}$: A Photomagnetic High-Spin Molecule. *Angew. Chem. Int. Ed.* **2004**, *43*, 5468–5471.

[4] Oshio, H.; Hoshino, N.; Ito, T.; Nakano, M. Single-Molecule Magnets of Ferrous Cubes: Structurally Controlled Magnetic Anisotropy. *J. Am. Chem. Soc.* **2004**, *126*, 8805–8812.

[5] Milios, C. J.; Vinslava, A.; Wernsdorfer, W.; Moggach, S.; Parsons, S.; Perlepes, S. P.; Christou, G.; Brechin, E. K. A Record Anisotropy Barrier for a Single-Molecule Magnet. *J. Am. Chem. Soc.* **2007**, *129*, 2754–2755.

[6] Freedman, D. E.; Harman, W. H.; Harris, T. D.; Long, G. J.; Chang, C. J.; Long, J. R. Slow Magnetic Relaxation in a High-Spin Iron(II) Complex. *J. Am. Chem. Soc.* **2010**, *132*, 1224–1225.

[7] Zhu, Y.-Y.; Cui, C.; Zhang, Y.-Q.; Jia, J.-H.; Guo, X.; Gao, C.; Qian, K.; Jiang, S.-D.; Wang, B.-W.; Wang, Z.-M. et al. Zero-Field Slow Magnetic Relaxation From Single Co(II) Ion: A Transition Metal Single-Molecule Magnet With High Anisotropy Barrier. *Chem. Sci.* **2013**, *4*, 1802–1806.

[8] Pineider, F.; Mannini, M.; Danieli, C.; Armelao, L.; Piras, F. M.; Magnani, A.; Cornia, A.; Sessoli, R. Deposition of Intact Tetrairon(III) Single Molecule Magnet Monolayers on Gold: An STM, XPS, and ToF-SIMS Investigation. *J. Mater. Chem.* **2010**, *20*, 187–194.

[9] Gonidec, M.; Biagi, R.; Corradini, V.; Moro, F.; Renzi, V. D.; del Pennino, U.; Summa, D.; Muccioli, L.; Zannoni, C.; Amabilino, D. B. et al. Surface Supramolecular Organization of a Terbium(III) Double-Decker Complex on Graphite and its Single Molecule Magnet Behavior. *J. Am. Chem. Soc.* **2011**, *133*, 6603–6612.

[10] Wende, H.; Bernien, M.; Luo, J.; Sorg, C.; Ponpandian, N.; Kurde, J.; Miguel, J.; Piantek, M.; Xu, X.; Eckhold, P. et al. Substrate-Induced Magnetic Ordering and Switching of Iron Porphyrin Molecules. *Nat. Mater.* **2007**, *6*, 516–520.

[11] Ali, M. E.; Sanyal, B.; Oppeneer, P. M. Tuning the Magnetic Interaction Between Manganese Porphyrins and Ferromagnetic Co Substrate Through Dedicated Control of the Adsorption. *J. Phys. Chem. C* **2009**, *113*, 14381–14383.

[12] Bernien, M.; Miguel, J.; Weis, C.; Ali, M. E.; Kurde, J.; Krumme, B.; Panchmatia, P. M.; Sanyal, B.; Piantek, M.; Srivastava, P. et al. Tailoring the Nature of Magnetic Coupling of Fe-Porphyrin Molecules to Ferromagnetic Substrates. *Phys. Rev. Lett.* **2009**, *102*, 047202.

[13] Bhandary, S.; Brena, B.; Panchmatia, P. M.; Brumboiu, I.; Bernien, M.; Weis, C.; Krumme, B.; Etz, C.; Kuch, W.; Wende, H. et al. Manipulation of Spin State of Iron Porphyrin by Chemisorption on Magnetic Substrates. *Phys. Rev. B* **2013**, *88*, 024401.

[14] Matsuda, K.; Irie, M. A Diarylethene With Two Nitronyl Nitroxides: Photoswitching of Intramolecular Magnetic Interaction. *J. Am. Chem. Soc.* **2000**, *122*, 7195–7201.

[15] Lin, P.-H.; Burchell, T.; Ungur, L.; Chibotaru, L.; Wernsdorfer, W.; Murugesu, M. A Polynuclear Lanthanide Single-Molecule Magnet With a Record Anisotropic Barrier. *Angew. Chem. Int. Ed.* **2009**, *48*, 9489–9492.

[16] Mannini, M.; Pineider, F.; Danieli, C.; Totti, F.; Sorace, L.; Sainctavit, P.; Arrio, M.-A.; Otero, E.; Joly, L.; Cezar, J. C. et al. Quantum Tunnelling of the Magnetization in a Monolayer of Oriented Single-Molecule Magnets. *Nature* **2010**, *468*, 417–421.

[17] Yamaguchi, K.; Morishima, I. Low-Valent Iron Porphyrins. NMR Evidence for π-Anion-Radical Character in Two-Electron-Reduced Iron(III) Meso- or β-Pyrrole-Substituted Porphyrins. *Inorg. Chem.* **1992**, *31*, 3216–3222.

[18] Auwärter, W.; Écija, D.; Klappenberger, F.; Barth, J. V. Porphyrins at Interfaces. *Nat. Chem.* **2015**, *7*, 105–120.

[19] Gottfried, J. M. Surface Chemistry of Porphyrins and Phthalocyanines. *Surf. Sci. Rep.* **2015**, *70*, 259–379.

[20] Wäckerlin, C.; Chylarecka, D.; Kleibert, A.; Müller, K.; Iacovita, C.; Nolting, F.; Jung, T. A.; Ballav, N. Controlling Spins in Adsorbed Molecules by a Chemical Switch. *Nat. Commun.* **2010**, *1*, 61.

[21] Miguel, J.; Hermanns, C. F.; Bernien, M.; Krüger, A.; Kuch, W. Reversible Manipulation of the Magnetic Coupling of Single Molecular Spins in Fe-Porphyrins to a Ferromagnetic Substrate. *J. Phys. Chem. Lett.* **2011**, *2*, 1455–1459.

[22] Hermanns, C. F.; Bernien, M.; Krüger, A.; Miguel, J.; Kuch, W. Switching the Electronic Properties of Co-Octaethylporphyrin Molecules on Oxygen-Covered Ni Films by NO Adsorption. *J. Phys.: Condens. Matter* **2012**, *24*, 394008.

[23] Wäckerlin, C.; Tarafder, K.; Siewert, D.; Girovsky, J.; Hählen, T.; Iacovita, C.; Kleibert, A.; Nolting, F.; Jung, T. A.; Oppeneer, P. M. et al. On-Surface Coordination Chemistry of Planar Molecular Spin Systems: Novel Magnetochemical Effects Induced by Axial Ligands. *Chem. Sci.* **2012**, *3*, 3154–3160.

[24] Wäckerlin, C.; Tarafder, K.; Girovsky, J.; Nowakowski, J.; Hählen, T.; Shchyrba, A.; Siewert, D.; Kleibert, A.; Nolting, F.; Oppeneer, P. M. et al. Ammonia Coordination Introducing a Magnetic Moment in an On-Surface Low-Spin Porphyrin. *Angew. Chem. Int. Ed.* **2013**, *52*, 4568–4571.

[25] Di Santo, G.; Blankenburg, S.; Castellarin-Cudia, C.; Fanetti, M.; Borghetti, P.; Sangaletti, L.; Floreano, L.; Verdini, A.; Magnano, E.; Bondino, F. et al. Supramolecular Engineering Through Temperature-Induced Chemical Modification of 2H-Tetraphenylporphyrin on Ag(111): Flat Phenyl Conformation and Possible Dehydrogenation Reactions. *Chem. Eur. J.* **2011**, *17*, 14354–14359.

[26] Röckert, M.; Franke, M.; Tariq, Q.; Ditze, S.; Stark, M.; Uffinger, P.; Wechsler, D.; Singh, U.; Xiao, J.; Marbach, H. et al. Coverage- and Temperature-Dependent Metalation and Dehydrogenation of Tetraphenylporphyrin on Cu(111). *Chem. Eur. J.* **2014**, *20*, 8948–8953.

[27] Liu, B.; Fu, H.; Guan, J.; Shao, B.; Meng, S.; Guo, J.; Wang, W. An Iron-Porphyrin Complex With Large Easy-Axis Magnetic Anisotropy on Metal Substrate. *ACS Nano* **2017**, *11*, 11402–11408.

[28] Rau, I. G.; Baumann, S.; Rusponi, S.; Donati, F.; Stepanow, S.; Gragnaniello, L.; Dreiser, J.; Piamonteze, C.; Nolting, F.; Gangopadhyay, S. et al. Reaching the Magnetic Anisotropy Limit of a 3d Metal Atom. *Science* **2014**, *344*, 988–992.

[29] Hirjibehedin, C. F.; Lin, C.-Y.; Otte, A. F.; Ternes, M.; Lutz, C. P.; Jones, B. A.; Heinrich, A. J. Large Magnetic Anisotropy of a Single Atomic Spin Embedded in a Surface Molecular Network. *Science* **2007**, *317*, 1199–1203.

[30] Heinrich, B. W.; Braun, L.; Pascual, J. I.; Franke, K. J. Tuning the Magnetic Anisotropy of Single Molecules. *Nano Lett.* **2015**, *15*, 4024–4028.

[31] Bryant, B.; Spinelli, A.; Wagenaar, J. J. T.; Gerrits, M.; Otte, A. F. Local Control of Single Atom Magnetocrystalline Anisotropy. *Phys. Rev. Lett.* **2013**, *111*, 127203.

[32] Gambardella, P.; Stepanow, S.; Dmitriev, A.; Honolka, J.; de Groot, F. M. F.; Lingenfelder, M.; Gupta, S. S.; Sarma, D. D.; Bencok, P.; Stanescu, S. et al. Supramolecular Control of the Magnetic Anisotropy In Two-dimensional High-Spin Fe Arrays at a Metal Interface. *Nat. Mater.* **2009**, *8*, 189–193.

[33] Grill, L.; Dyer, M.; Lafferentz, L.; Persson, M.; Peters, M. V.; Hecht, S. Nano-Architectures by Covalent Assembly of Molecular Building Blocks. *Nat. Nanotechnol.* **2007**, *2*, 687–691.

[34] Heinrich, B. W.; Ahmadi, G.; Müller, V. L.; Braun, L.; Pascual, J. I.; Franke, K. J. Change of the Magnetic Coupling of a Metal–Organic Complex With the Substrate by a Stepwise Ligand Reaction. *Nano Lett.* **2013**, *13*, 4840–4843.

[35] Franc, G.; Gourdon, A. Covalent Networks Through On-Surface Chemistry in Ultra-high Vacuum: State-of-the-Art and Recent Developments. *Phys. Chem. Chem. Phys.* **2011**, *13*, 14283–14292.

[36] Lackinger, M.; Heckl, W. M. A STM Perspective on Covalent Intermolecular Coupling Reactions on Surfaces. *J. Phys. D: Appl. Phys.* **2011**, *44*, 464011.

[37] Lepper, M.; Zhang, L.; Stark, M.; Ditze, S.; Lungerich, D.; Jux, N.; Hieringer, W.; Steinrück, H.-P.; Marbach, H. Role of Specific Intermolecular Interactions for the Arrangement of Ni(II)-5, 10, 15, 20-Tetraphenyltetrabenzoporphyrin on Cu(111). *J. Phys. Chem. C* **2015**, *119*, 19897–19905.

[38] Williams, C. G.; Wang, M.; Skomski, D.; Tempas, C. D.; Kesmodel, L. L.; Tait, S. L. Dehydrocyclization of Peripheral Alkyl Groups in Porphyrins at Cu(100) and Ag(111) Surfaces. *Surf. Sci.* **2016**, *653*, 130–137.

[39] Cirera, B.; Giménez-Agulló, N.; Björk, J.; Martínez-Peña, F.; Martin-Jimenez, A.; Rodriguez-Fernandez, J.; Pizarro, A. M.; Otero, R.; Gallego, J. M.; Ballester, P. et al. Thermal Selectivity of Intermolecular Versus Intramolecular Reactions on Surfaces. *Nat. Commun.* **2016**, *7*, 11002.

[40] Heim, D.; Écija, D.; Seufert, K.; Auwärter, W.; Aurisicchio, C.; Fabbro, C.; Bonifazi, D.; Barth, J. V. Self-Assembly of Flexible One-Dimensional Coordination Polymers on Metal Surfaces. *J. Am. Chem. Soc.* **2010**, *132*, 6783–6790.

[41] Lafferentz, L.; Eberhardt, V.; Dri, C.; Africh, C.; Comelli, G.; Esch, F.; Hecht, S.; Grill, L. Controlling On-Surface Polymerization by Hierarchical and Substrate-Directed Growth. *Nat. Chem.* **2012**, *4*, 215–220.

[42] Gao, H.-Y.; Wagner, H.; Zhong, D.; Franke, J.-H.; Studer, A.; Fuchs, H. Glaser Coupling at Metal Surfaces. *Angew. Chem. Int. Ed.* **2013**, *52*, 4024–4028.

[43] Flechtner, K.; Kretschmann, A.; Steinrück, H.-P.; Gottfried, J. M. NO-Induced Reversible Switching of the Electronic Interaction between a Porphyrin-Coordinated Cobalt Ion and a Silver Surface. *J. Am. Chem. Soc.* **2007**, *129*, 12110–12111.

[44] Hieringer, W.; Flechtner, K.; Kretschmann, A.; Seufert, K.; Auwärter, W.; Barth, J. V.; Görling, A.; Steinrück, H.-P.; Gottfried, J. M. The Surface Trans Effect: Influence of Axial Ligands on the Surface Chemical Bonds of Adsorbed Metalloporphyrins. *J. Am. Chem. Soc.* **2011**, *133*, 6206–6222.

[45] Isvoranu, C.; Wang, B.; Ataman, E.; Knudsen, J.; Schulte, K.; Andersen, J. N.; Bocquet, M.-L.; Schnadt, J. Comparison of the Carbonyl and Nitrosyl Complexes Formed by Adsorption of CO and NO on Monolayers of Iron Phthalocyanine on Au(111). *J. Phys. Chem. C* **2011**, *115*, 24718–24727.

[46] Ballav, N.; Wäckerlin, C.; Siewert, D.; Oppeneer, P. M.; Jung, T. A. Emergence of On-Surface Magnetochemistry. *J. Phys. Chem. Lett.* **2013**, *4*, 2303–2311.

[47] Thole, B. T.; Carra, P.; Sette, F.; van der Laan, G. X-Ray Circular Dichroism as a Probe of Orbital Magnetization. *Phys. Rev. Lett.* **1992**, *68*, 1943–1946.

[48] Carra, P.; Thole, B. T.; Altarelli, M.; Wang, X. X-ray Circular Dichroism and Local Magnetic Fields. *Phys. Rev. Lett.* **1993**, *70*, 694–697.

[49] Šipr, O.; Minár, J.; Ebert, H. On the Importance of the Magnetic Dipole Term T_Z in Analyzing X-Ray Magnetic Circular Dichroism Spectra of Clusters. *Europhys. Lett.* **2009**, *87*, 67007.

[50] van Vörden, D.; Lange, M.; Schmuck, M.; Schaffert, J.; Cottin, M. C.; Bobisch, C. A.; Möller, R. Communication: Substrate Induced Dehydrogenation: Transformation of Octa-Ethyl-Porphyrin Into Tetra-Benzo-Porphyrin. *J. Chem. Phys.* **2013**, *138*, 211102.

[51] Perdew, J. P.; Burke, K.; Ernzerhof, M. Generalized Gradient Approximation Made Simple. *Phys. Rev. Lett.* **1996**, *77*, 3865–3868.

[52] Kresse, G.; Furthmüller, J. Efficiency of Ab-Initio Total Energy Calculations for Metals and Semiconductors Using a Plane-Wave Basis Set. *Comput. Mater. Sci.* **1996**, *6*, 15–50.

[53] Grimme, S. Semiempirical GGA-Type Density Functional Constructed With a Long-Range Dispersion Correction. *J. Comput. Chem.* **2006**, *27*, 1787–1799.

[54] Dudarev, S. L.; Botton, G. A.; Savrasov, S. Y.; Humphreys, C. J.; Sutton, A. P. Electron-Energy-Loss Spectra and the Structural Stability of Nickel Oxide: An LSDA+U Study. *Phys. Rev. B* **1998**, *57*, 1505–1509.

[55] Panchmatia, P. M.; Sanyal, B.; Oppeneer, P. M. GGA+U Modeling of Structural, Electronic, and Magnetic Properties of Iron Porphyrin-Type Molecules. *Chem. Phys.* **2008**, *343*, 47–60.

[56] Ali, M. E.; Sanyal, B.; Oppeneer, P. M. Electronic Structure, Spin-States, and Spin-Crossover Reaction of Heme-Related Fe-Porphyrins: A Theoretical Perspective. *J. Phys. Chem. B* **2012**, *116*, 5849–5859, PMID: 22512398.

[57] Blöchl, P. E. Projector Augmented-Wave Method. *Phys. Rev. B* **1994**, *50*, 17953–17979.

[58] Monkhorst, H. J.; Pack, J. D. Special Points for Brillouin-Zone Integrations. *Phys. Rev. B* **1976**, *13*, 5188–5192.

[59] Girovsky, J.; Nowakowski, J.; Ali, M. E.; Baljozovic, M.; Rossmann, H. R.; Nijs, T.; Aeby, E. A.; Nowakowska, S.; Siewert, D.; Srivastava, G. et al. Long-range ferrimagnetic order in a two-dimensional supramolecular Kondo lattice. *Nat. Commun.* **2017**, *8*, 15388.

[60] Minamitani, E.; Tsukahara, N.; Matsunaka, D.; Kim, Y.; Takagi, N.; Kawai, M. Symmetry-Driven Novel Kondo Effect in a Molecule. *Phys. Rev. Lett.* **2012**, *109*.

[61] Piamonteze, C.; Miedema, P.; de Groot, F. M. F. Accuracy of the Spin Sum Rule in XMCD for the Transition-Metal L Edges From Manganese to Copper. *Phys. Rev. B* **2009**, *80*, 184410.

[62] Stepanow, S.; Miedema, P. S.; Mugarza, A.; Ceballos, G.; Moras, P.; Cezar, J. C.; Carbone, C.; de Groot, F. M. F.; Gambardella, P. Mixed-Valence Behavior and Strong Correlation Effects of Metal Phthalocyanines Adsorbed on Metals. *Phys. Rev. B* **2011**, *83*, 220401.